Scattering of 80-Mev π^- Mesons by Complex Nuclei*

W. F. BAKER AND J. RAINWATER, *Columbia University, New York, New York*

AND

R. E. WILLIAMS, *Paul Rosenberg Associates, Mount Vernon, New York*

(Received August 4, 1958)

The elastic scattering of 80-Mev π^- mesons by lithium, carbon, aluminum, and copper has been investigated using a π^- detector which gives improved discrimination against low-energy-loss inelastic events. A "transmission" scatterer orientation was necessary to maintain energy resolution, so only less than 120° scattering was studied. The new differential scattering cross sections for lithium, aluminum, and copper agree with the previously reported results at small angles but are 2 to 10 times smaller at larger angles. There are indications of diffraction structure in aluminum and copper which were not previously observed due to the poorer energy resolution of the earlier measurements.

Including the incident beam energy spread, the detector sensitivity is down by factors of 3 and 9 for $E\pm5.0$ Mev and $E\pm10$ Mev when peaked for mean energy E. This was used to separate the scattering from carbon into elastic and inelastic components for excitation of the 4.43 and (7.65 and 9.61) Mev levels. Inelastic scatterings from lithium have also been studied. For the same momentum transfer on scattering, the ratio of the inelastic scattering with excitation to the 4.43-Mev and 9.61-Mev levels to the elastic differential scattering cross section is the same, within experimental accuracy, as found by Fregeau for the scattering of 187-Mev electrons on carbon. The elastic scattering is compared with the results of complex square-well phase shift calculations, and with diffuse-edge optical model and modified Kisslinger model calculations.

I. INTRODUCTION

THE angular distributions of the scattering of 80-Mev π^- mesons by lithium, carbon, aluminum, and copper have been investigated using a counter system with an energy resolution considerably improved over that previously used in this laboratory.[1–3] This was done by counting only those mesons stopping in a counter, whereas in the earlier work a differential range method was used which offered poorer discrimination against inelastic scatterings. This latter method had the advantage of functioning identically for π^- and π^+ scattering; however, the energy resolution was not sufficient to separate the elastic scattering from the inelastic scatterings with energy losses up to about 10 Mev. This fact was particularly troublesome in aluminum[1] and copper[3] where the predicted diffraction patterns were not visible. Optical model phase shift calculations were made[3,4] using a complex square well; these could be matched well with the experimental results at small angles and were not inconsistent with the results at large angles considering the energy resolution of the apparatus. In view of the improved energy resolution now available, the elastic scattering from lithium, aluminum, and copper was reexamined. In addition to measuring the elastic cross sections for carbon, the energy distribution of the scattered beam was investigated at a few angles to determine approximate inelastic scattering cross sections for excitation of the low-lying levels.

The first work on π^- nucleus interactions of Bernardini *et al.*[5,6] used photographic emulsions and presented the elastic scattering in terms of total cross sections. A number of cloud chamber investigations have been made of the angular distributions of pions scattered by complex nuclei. Byfield, Kessler, and Lederman examined π^+ and π^- interactions with carbon at 62-Mev[7] and π^- with lead and carbon at 125 Mev.[8] Saphir[9] measured π^+ on lead at 50 Mev; Dzhelepov *et al.*,[10] π^- on carbon and lead at 230 and 250 Mev, respectively. These experiments were not designed solely for elastic scattering measurements and lacked the resolution which could be realized with counter techniques.

Stork,[11] using a counter defining a fixed annular region, measured π^+ scattering from various nuclei at 33, 46, and 68 Mev. His results were consistent with earlier work and were not inconsistent with the complex square-well optical model.

In addition to the improved energy resolution in the present experiment, relatively good angular resolution, <6°, and statistical accuracy, ~10%, have been obtained in order to see details in the angular distribution more clearly than was possible in the earlier work using emulsions and cloud chambers.

At 80 Mev, the energy of the π's used in this experiment, nucleon data[12] show the π^-+p elastic cross

* This research is supported by the Office of Naval Research and the U. S. Atomic Energy Commission.

1 Pevsner, Rainwater, Williams, and Lindenbaum, Phys. Rev. **100**, 1419 (1955).

2 Williams, Rainwater, and Pevsner, Phys. Rev. **101**, 412 (1956).

3 Williams, Baker, and Rainwater, Phys. Rev. **104**, 1695 (1956).

4 A. Pevsner and J. Rainwater, Phys. Rev. **100**, 1431 (1955).

5 Bernardini, Booth, Lederman, and Tinlot, Phys. Rev. **82**, 105 (1951).

6 Bernardini, Booth, and Lederman, Phys. Rev. **83**, 1075 and 1277 (1951).

7 Byfield, Kessler, and Lederman, Phys. Rev. **36**, 17 (1952).

8 J. O. Kessler and L. M. Lederman, Phys. Rev. **94**, 689 (1954).

9 G. Saphir, Phys. Rev. **104**, 535 (1956).

10 Dzhelepov, Xvanov, Kozodaev, Osipenko, Petrov, and Russkov, *Proceedings of the CERN Symposium on High-Energy Accelerators and Pion Physics, Geneva, 1956* (European Organization of Nuclear Research, Geneva, 1956), Vol. 2, p. 314.

11 D. H. Stork, Phys. Rev. **93**, 868 (1954).

12 See H. Bethe and F. de Hoffmann, *Mesons and Fields* (Row, Peterson and Company, Evanston, 1955), Vol. 2, Sec. 29 for a review of the experimental results and theoretical interpretation.

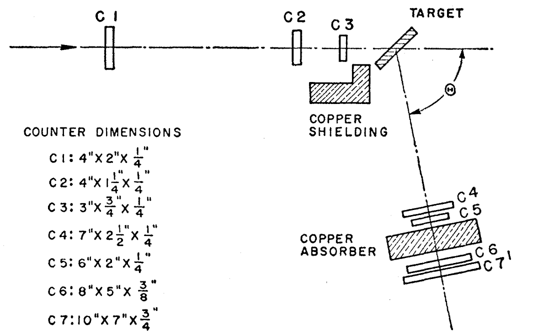

FIG. 1. Counter arrangement.

section to be down by about a factor of five from the $\pi^+ + p$ cross section. On the basis of charge symmetry the scattering of π^-'s would be principally dependent on the neutrons distributed in the nucleus. The possibility of a larger radius for the neutron distribution than for the proton distribution in heavier nuclei has been suggested by Johnson and Teller.[13] Courant[14] pointed out that this could be investigated by measuring the π^+ and π^- interaction cross sections for lead at 700 Mev where the $\pi^+ + n$ interaction is about $2\frac{1}{2}$ times the $\pi^+ + p$. Abashian, Cool, and Cronin[15] carried out such an experiment, and the data show no evidence for a larger radius of the neutron distribution. The dependence of π^+ scattering on nuclear radius, therefore, should be no different than for the π^- scattering examined here except for Coulomb effects.

II. EXPERIMENTAL EQUIPMENT

The mesons used in these measurements were produced when the 380-Mev proton beam of the Nevis cyclotron struck an internal beryllium target. From the continuous energy distribution thus produced, those mesons of the desired momentum were selected by the fringing field of the cyclotron magnet to pass through a channel in the shielding wall and out into the experimental area. Upon leaving this channel the mesons were deflected slightly from the raw beam by a magnet which also focused the beam vertically, defocused it horizontally, and improved further the energy resolution.

Beyond the magnet was placed the scattering stand, the significant parts of which are shown in Fig. 1. Counters 1, 2, and 3 defined the incident beam; the smallest of these, counter 3, established the target size. Counters 4, 5, 6, and 7′ in conjunction with the copper absorber formed a telescope for detection of the scattered particles. The scattering stand was remotely controlled from the adjacent laboratory building, so that the angle of scattering, θ, and the copper absorber thickness could be varied, and so that the target could be removed for background measurements. The target holder was coupled to the scattered beam detection telescope in such a way as to rotate through half the angle of scattering. The frame of the stand is far enough from the counters to cut down background due to scattering in the frame.

The principal improvement in this experiment as compared to the earlier work[1–3] was in the energy resolution for detection of the scattered π's. This was accomplished by counting only those π's stopping in a given counter, thus giving rise to the large pulses associated with stars. This method, of course, limited the measurements to the scattering of negative π mesons. Counter 6, shown in Fig. 1, was the stopping counter which was operated with the voltage on its phototubes low enough so as to count only the stoppings. Counter 7′ discriminated against mesons which were slightly more energetic than those we wished to count and was particularly necessary when measuring inelastic scatterings. A meson which stopped in 7′ would be near the end of its range in 6 and would be heavily ionizing there; it might, therefore, have been counted by 6. Since we did not wish to count such a particle counter 7′, which was appreciably larger in area than 6, was placed in anticoincidence with 6. Thus only π^- mesons were counted which had an energy sufficient to penetrate the copper absorber but not enough to get through counter 6.

Counter 5 was the smallest counter in the scattered beam detection telescope and therefore determined both the solid angle and linear angle subtended by the telescope.

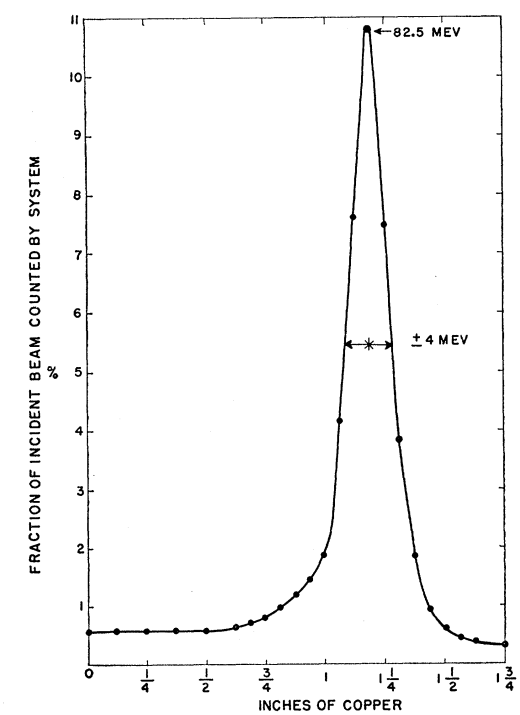

FIG. 2. Incident beam range curve.

[13] M. H. Johnson and E. Teller, Phys. Rev. 93, 357 (1954).
[14] E. D. Courant, Phys. Rev. 94, 1081 (1954).
[15] Abashian, Cool, and Cronin, Phys. Rev. 104, 855 (1956).

To determine the energy of the incident beam the scattered beam detection telescope was placed in the incident beam at the target position and a range curve taken. Such a range curve is shown by Fig. 2. The desired energy was obtained by first positioning the cyclotron target as closely as possible and then making fine adjustments by varying the cyclotron magnetic field to give the range curve peak at an absorber thickness corresponding to 82.5 Mev. Since the scattering targets had a thickness equivalent to a 5-Mev energy loss this would then correspond to 80 Mev at the center of the target. This technique was very sensitive to the field strength of the cyclotron magnet and was greatly facilitated by the recent installation of a mechanical rectifier to provide stable current for the cyclotron magnet. A 1% change in cyclotron magnet current gave an appreciable change in the ratio of the points on either side of the peak in Fig. 2.

The half-width at half-maximum of the energy resolution of the system, including the incident beam energy spread is seen from Fig. 2 to be 4 Mev. After correcting for straggling in the absorber and for the thickness of the stopping counter, *C*6, this corresponds to an incident beam energy spread of ± 3 Mev. The energy spread was decreased somewhat by blocking down the channel opening in the cyclotron shielding wall. The flat portion of the range curve below the peak is mainly due to stars produced in flight.

In Fig. 1 the target is shown in the transmission position which was used throughout in this experiment. With the normal to the target bisecting the angle of scattering all particles will have the same path length in the target regardless of the point of scattering. In particular, all elastically scattered mesons will have the same energy loss in the target. To measure scattering through angles greater than about 120° it would be necessary to change the target to a reflection orientation perpendicular to the transmission position shown. A particle scattered from a target in such a reflection position could have a path length in the target of from zero to more than twice the thickness of the target. Since the targets all had a thickness corresponding to a 5-Mev loss for π's at 80 Mev, the energy resolution of the system would be destroyed. We therefore limited our measurements to scatterings through angles less than 120°.

Background was considerably reduced by the insertion of copper shielding as shown in Fig. 1. This shielded the scattered beam detection telescope from particles which were scattered in the scintillator of counter 3, which had previously contributed most of the background.

The seven counters were made of plastic scintillating material each being viewed by two 1P21 photomultiplier tubes. The deflecting magnet focused the beam into a thin horizontal line at the target position, and the scattering was measured in a vertical plane defined by a rotation about this line as an axis. Counter 3, the target defining counter, had its 3-in. edge parallel to the focussed line and its $\frac{3}{4}$-in. edge vertically perpendicular to it. All counters had their longest dimensions perpendicular to the plane of scattering.

In counters 1, 2, 3, 4, and 5 the outputs from the anodes of the two phototubes were connected in parallel. The resultant negative pulse was then limited, amplified, and clipped in the counter. Counters 6 and 7′ were electronically the same counter with the last dynodes of the phototubes of counter 7′ connected to the anodes of those of counter 6 to provide the necessary anticoincidence. Otherwise the circuitry was similar to the other five counters. Since the phototubes of counter 6 were not operated in the usual plateau region, a very well regulated high-voltage supply was necessary.

The pulses from the counters were fed through distributed amplifiers to "fast" coincidence circuits. These circuits were used to make coincidences among counters 1, 2, and 3; counters 1, 2, 3, 4, and 5; and counters 4, 5, 6, and 7′. (These coincidence circuits were similar to that of Garwin.[16]) The pulses were then shaped and a coincidence made between the 12345 and 4567′ pulses with a "slow" coincidence circuit. The resultant 1234567′ counts were then recorded on a scaler as were the 12345 and 4567′ pulses. The 123 counts being of a much higher rate, about 1.5×10^3/sec time average, were first scaled down with a ten-megacycle scaler and then recorded as the others were. The 123 and 1234567′ counts were the only ones utilized in these measurements; the 12345 and 4567′ counts were monitored as a check on the stability of the equipment as they were of a higher rate than the 1234567′ counts. The instantaneous counting rates during that part of the cyclotron fm cycle when protons strike the internal beryllium target are estimated to be about 20 to 50 times larger than the time average values.

III. EXPERIMENTAL PROCEDURE

In measuring the elastic differential cross section for a particular element at an angle, the thickness of the target and the energy loss for an elastic scattering were taken into account to determine the thickness of absorber equivalent to the peak point in the range curve of Fig. 2. The ratio of the relative number of counts thus obtained to the corresponding point of the incident beam range curve will be directly proportional to the desired cross section. The cross section thus measured will henceforth be called the "uncorrected elastic" cross section.

At a few selected angles for carbon and lithium, scattered beam range curves were taken using thicknesses of absorber equivalent, for an elastic scattering, to the thicknesses indicated by the black dots on the resolution (i.e., range) curve of Fig. 3. If the points so obtained had the same ratio to one another as the corresponding points for the incident beam, the scat-

[16] R. Garwin, Rev. Sci. Instr. **27**, 618 (1953).

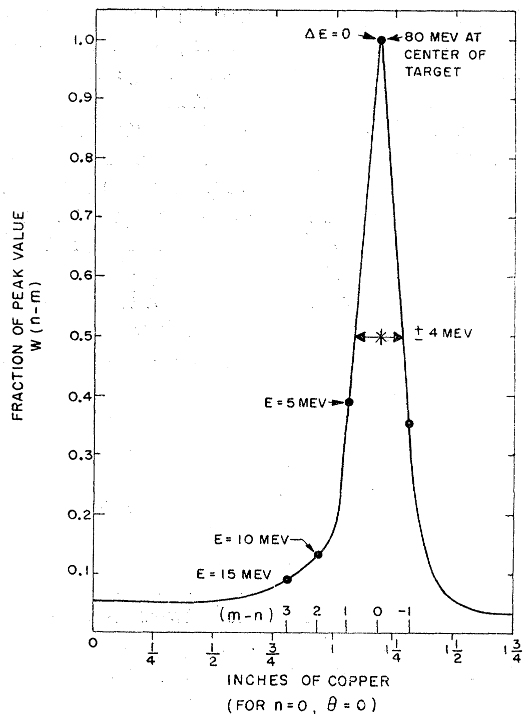

FIG. 3. Energy resolution of system.

tering was principally elastic. Inelastic scatterings, when present, were detected by a relative increase in the points on the low-energy side of the elastic peak.

For an absorber thickness giving a maximum rate for elastic scattering, the relative detection efficiency is lower by factors of about 0.35, 0.09, and 0.04 for inelastic scatterings with nuclear excitations of 5, 10, and 15 Mev, respectively. ($\frac{1}{8}$ in. copper change in range corresponds to ≈ 5 Mev meson energy change.) These factors are obtained from the height of the curve of Fig. 3 at points to the right of the peak by $\frac{1}{8}$ in., $\frac{1}{4}$ in., and $\frac{3}{8}$ in. of copper, respectively. For an absorber thickness giving a maximum response for a scattering involving 10-Mev nuclear excitation, the relative sensitivities are about 0.13, 0.39, 1.00, and 0.35 for scattering involving zero, 5-Mev, 10-Mev, and 15-Mev nuclear excitations. If it is assumed that all scatterings correspond to one of these four cases, the corrected differential cross sections for each such scattering can be determined by solving the following set of four simultaneous linear equations:

$$N_m = \sum_{n=0}^{3} W(m-n) F_n.$$

The meaning of the symbols may be understood as follows. Let C_m be the number of counts obtained when the absorber thickness is optimum for detecting scatterings involving $5m$ Mev nuclear excitation. We then calculate a differential cross section N_m using only C_m and assuming that all scatterings involved $5m$ Mev excitation (for each m). If the actual differential cross section for $5n$ Mev energy excitation is F_n, then the contribution of actual F_n to N_m is $W(m-n)F_n$ and each F_n contributes to given N_m. $W(m-n)$ is the relative sensitivity (Fig. 3) for detecting scatterings of $5n$ Mev loss using $(m/8)$ in. of copper less than for the elastic peak. We call the N_m the "uncorrected" cross sections and the F_n the "corrected" cross sections. The simultaneous linear equations must be solved for the F_n, given the N_m and $W(m-n)$.

The above analysis does not correspond to reality in that nuclear levels do not just occur at 5, 10, and 15 Mev above the ground state. Since the equations are linear, however, the effect on N_0, N_1, N_2, and N_3 of many levels at arbitrary energies can be represented as if only contributions for integer n were present. For an arbitrary element having levels at $(n_j+\alpha_j)$ 5 Mev (for the jth level, $0 \leq \alpha_j < 1$), the F_n determined from the analysis will receive contributions from all excited states within 5 Mev of $5n$ Mev excitation, with a relative weighting for a given $F_{n\pm\alpha_j}$ of $\sinh[(1-\alpha_j)p]/\sinh p$, when the resolution function is approximated by

$$W(m-n) \approx e^{-|m-n|p}.$$

The actual curve of Fig. 3 is not exactly of the form $e^{-|m-n|p}$, but it approximates it fairly closely on the high side (i.e., for $n > m$). The slower drop for larger absorber thickness in Fig. 3 may represent some contribution from μ mesons and electrons which will be

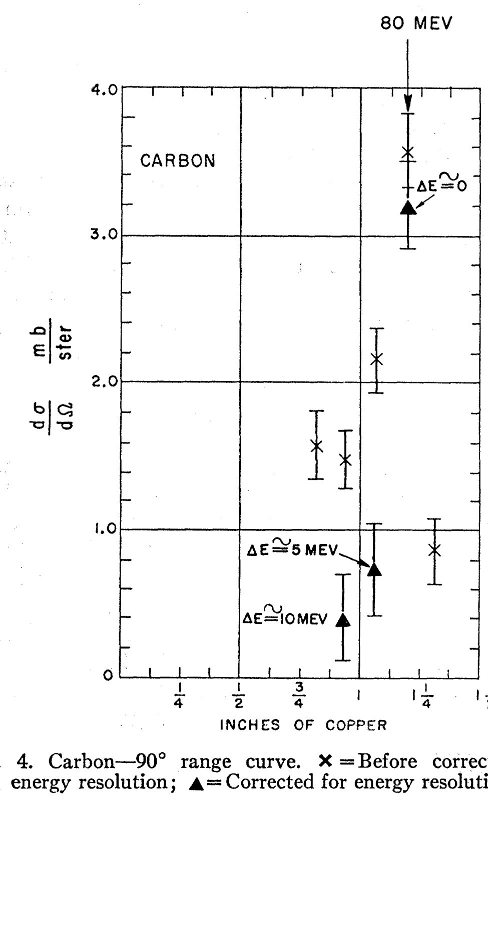

FIG. 4. Carbon—90° range curve. × = Before correcting for energy resolution; ▲ = Corrected for energy resolution.

TABLE I. Energy distribution measurements at selected angles for carbon. $d\sigma/d\Omega$=uncorrected differential elastic cross section in millibarns per steradian; $(d\sigma/d\Omega)_0$=elastic cross section corrected for energy resolution; $(d\sigma/d\Omega)_5$=corrected inelastic cross section for energy loss≅5 Mev, etc.

θ_{lab}(deg)	$d\sigma/d\Omega$	$(d\sigma/d\Omega)_0$	$(d\sigma/d\Omega)_5$	$(d\sigma/d\Omega)_{10}$	$(d\sigma/d\Omega)_{15}$
40±3.7	39.0±1.4	39.1±1.6	−0.39±1.40	−0.04±1.19	−0.25±1.21
70±5.6	2.92±0.22	2.78±0.27	0.25±0.35	−0.19±0.35	1.12±0.32
90±5.6	3.58±0.25	3.21±0.30	0.74±0.32	0.41±0.30	1.05±0.28
110±5.6	2.55±0.16	1.65±0.20	2.28±0.28	0.69±0.28	1.97±0.27

relatively absent in the scattered beam. In examining the contribution to the "uncorrected elastic" point N_0 due to inelastic scatterings, only this $n>m$ region contributes. Thus the analysis would be expected to be fairly reliable for evaluating F_0 when the inelastic scattering is less than or not considerably greater than the elastic scattering. The $W(m-n)$ used is that of Fig. 3 rather than $e^{-|m-n|p}$, which was only introduced for purposes of discussion.

Carbon is particularly well suited to this type of energy distribution examination, since it has its first excited level at 4.43 Mev and its next two levels at 7.65 and 9.61 Mev. Thus for carbon we attribute with good accuracy the corrected elastic cross section F_0 to purely elastic scattering, and we associate the first inelastic cross section F_1 mainly with scatterings which excite the nucleus to the 4.43-Mev level. Although the 7.65-Mev level would also contribute to F_1, measurements[17] of the inelastic scattering of 187-Mev electrons on carbon show its contribution there to be negligible relative to the 4.43-Mev level contribution. The next inelastic cross section, F_2, we attribute to excitation of the 7.65 Mev, 9.61 Mev, and higher levels. The electron scattering results indicate much greater contributions from the 9.61-Mev level than the 7.65-Mev level. This should probably also apply here.

In the case of lithium F_0 is due to a combination of true elastic scattering and excitation of the 0.48-Mev level. The first and second inelastic cross sections F_1 and F_2 we associate with the 4.61-Mev and higher levels.

The principal purpose of this experiment was to measure elastic cross sections, therefore this technique was applied at only a few selected angles for carbon and lithium, and the necessary corrections to the elastic cross sections for intermediate angles were obtained by interpolation.

"Uncorrected elastic" cross sections were also measured for aluminum and copper.

IV. EXPERIMENTAL RESULTS

Energy distribution measurements were made for the negative π's scattered from carbon at 40°, 70°, 90°, and 110°. The results are listed in Table I and shown in Fig. 4 for 90°. It should be noted that the N_0, F_0, F_1, F_2, and F_3 of the discussion in the previous section are $(d\sigma/d\Omega)$, $(d\sigma/d\Omega)_0$, $(d\sigma/d\Omega)_5$, $(d\sigma/d\Omega)_{10}$, and $(d\sigma/d\Omega)_{15}$, respectively, in the tables. The energy resolution function is shown in Fig. 3 which is identical in form to the incident beam range curve of Fig. 2. At 90° the points on the low-energy side of the elastic peak are high relative to the incident beam because of some inelastic contribution. The corrected elastic cross section is seen to be slightly smaller than the uncorrected elastic value, and the inelastic cross sections are significant.

The "uncorrected elastic" cross sections for carbon and the corrected elastic cross sections are listed in Table II as a function of angle. The linear angular resolution listed there is a combination of the angle subtended by the scattered beam detection telescope, the angular spread of the incident meson beam, and small-angle multiple Coulomb scattering in the target. The angular distribution of the corrected elastic cross sections and the inelastic cross sections at 40°, 70°, 90°, and 110° are shown in Fig. 5.

For lithium, energy distribution measurements were made at 70° and 110° and are listed in Table III. The "uncorrected elastic" cross sections are listed in Table IV, and these as well as the corrected elastic and first

TABLE II. Uncorrected and corrected differential elastic cross sections in millibarns per steradian for carbon.

θ_{lab}(deg)	$d\sigma/d\Omega$	$(d\sigma/d\Omega)_0$
20±3.0	150±15	150±15
20±3.4	147±17	147±17
25±3.4	123±11	123±11
30±3.4	73.7±5.4	73.7±5.4
35±3.4	67.3±6.0	67.3±6.0
35±3.7	63.8±6.1	63.8±6.1
40±3.7	39.0±1.4	39.1±1.6
45±3.7	29.0±2.3	29.0±2.4
50±3.7	18.8±3.0	18.6±3.1
50±4.1	19.2±2.6	19.0±2.7
55±4.1	12.5±1.7	12.2±1.8
60±4.1	5.44±1.43	5.28±1.50
60±5.6	6.69±0.98	6.50±1.10
65±5.6	3.41±0.53	3.28±0.60
70±5.6	2.92±0.22	2.78±0.27
75±5.6	3.53±0.59	3.33±0.65
80±5.6	3.12±0.40	2.92±0.45
85±5.6	3.47±0.56	3.22±0.60
90±5.6	3.59±0.25	3.21±0.30
95±5.6	3.67±0.55	3.19±0.60
100±5.6	3.41±0.41	2.84±0.50
105±5.6	3.30±0.50	2.58±0.55
110±5.6	2.55±0.16	1.65±0.20
$116\frac{2}{3}$±5.6	2.73±0.53	1.65±0.60

[17] J. H. Fregeau, Phys. Rev. **104**, 225 (1956). The theory of the excitation of the 4.43-, 7.65-, and 9.61-Mev levels in carbon by fast electrons is given by M. K. Pal and M. A. Nagarajan, Phys. Rev. **108**, 1577 (1957).

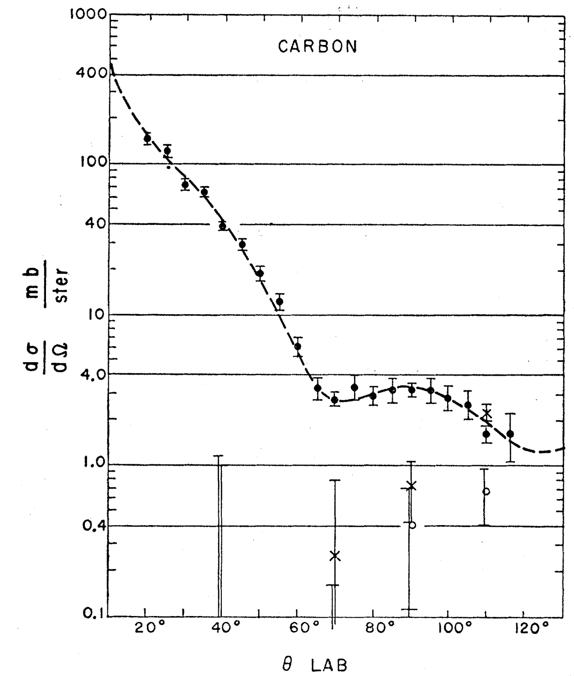

FIG. 5. 80 Mev π^- carbon scattering. ● Corrected elastic; × 5-Mev inelastic; ○ 10-Mev inelastic. Dashed curve is for modified Kisslinger model with $R_0=1.08A^{\frac{1}{3}}\times10^{-13}$ cm, $a=0.25\times10^{-13}$ cm, $C=-1.1-0.1i$, and $C'=+0.35-0.15i$.

inelastic cross sections at the above angles are shown in Fig. 6 as a function of laboratory scattering angle. The solid curve in Fig. 6 shows the previously published results of Williams *et al.*[2]

In the aluminum measurements an earlier version of counter 6 was used which had a scintillator $1\frac{1}{8}$ in. thick but which was identical in other respects to the counter 6 described under Experimental Procedure. The results of the aluminum measurements are listed in Table V and shown in Fig. 7. Evidences of some diffraction structure are now suggested as compared to the published results of Pevsner *et al.*[1] shown by the solid curve.

In the scattering from copper, shown in Table VI and Fig. 8, diffraction structure is evident with a minimum at 80° and a subsidiary maximum at 90°. The previous results of Williams *et al.*[3] are shown by the solid curve.

TABLE III. Energy distribution measurements at selected angles for lithium. $d\sigma/d\Omega$ = uncorrected differential elastic cross section in millibarns per steradian; $(d\sigma/d\Omega)_0$ = elastic cross section corrected for energy resolution; $(d\sigma/d\Omega)_5$ = corrected inelastic cross section for energy loss ≅ 5 Mev, etc.

θ_{lab}(deg)	$d\sigma/d\Omega$	$(d\sigma/d\Omega)_0$	$(d\sigma/d\Omega)_5$	$(d\sigma/d\Omega)_{10}$
70±5.5	0.99±0.13	0.80±0.16	0.48±0.26	0.20±0.23
110±5.5	3.25±0.32	2.57±0.40	1.29±0.62	1.42±0.63

TABLE IV. Uncorrected differential elastic cross sections for lithium in millibarns per steradian.

θ_{lab}(deg)	$d\sigma/d\Omega$	θ_{lab}(deg)	$d\sigma/d\Omega$
40±4.0	19.1±1.4	80±5.5	1.54±0.20
45±4.0	15.8±1.4	85±5.5	1.54±0.14
50±4.0	9.54±0.89	90±5.5	2.36±0.24
55±5.5	4.53±0.33	95±5.5	2.84±0.24
60±4.0	3.47±0.66	100±5.5	3.56±0.34
65±5.5	2.18±0.25	105±5.5	3.58±0.32
70±5.5	0.99±0.13	110±5.5	3.25±0.32
75±5.5	1.00±0.16		

V. DISCUSSION OF RESULTS

1. Inelastic to Elastic Scattering Ratios

A. Comparison with Earlier Measurements

A first obvious result of comparisons with earlier[1–3] measurements for Li, Al, and Cu is the lowering of the

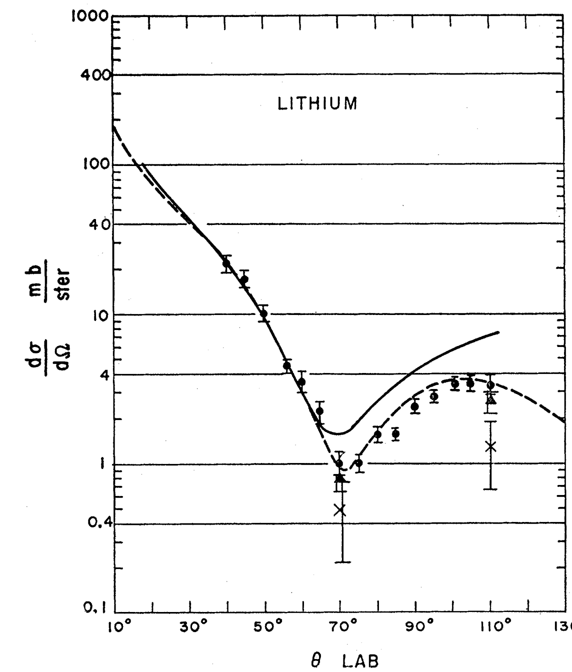

FIG. 6. 80-Mev π^- lithium scattering. ● Elastic before correcting for energy resolution; ▲ elastic corrected for energy resolution; × 5-Mev inelastic corrected for energy resolution. Solid curve is results of Williams *et al.*[3] Dashed curve is for Modified Kisslinger model with $R_0=1.08A^{\frac{1}{3}}\times10^{-13}$ cm, $a=0.25\times10^{-13}$ cm, $C=-1.3-0.15i$, and $C'=+0.3-0.15i$.

elastic differential cross section values for larger angles. This is to be expected as the energy resolution is improved and more or all of the scattering corresponding to excitation of the compound nucleus is eliminated. In the cases of Al and Cu such inelastic contributions are still present and the experimental points, within experimental uncertainties, should be interpreted as giving upper limits on the purely elastic (coherent) scattering. In the cases of Li and C, as discussed below, there is reason to believe that the true elastic scattering has been separated from that corresponding to nuclear excitation.

A comparison with the scattering of γ rays by bound electrons is of interest in estimating roughly the most likely excitation of the nucleus for a given scattering angle. Coherent x-ray scattering combines the scattering amplitudes from each of the bound electrons and is elastic with respect to the system as a whole. A form factor arises which represents the probability that the electron remain in its initial bound state after receiving the full momentum transfer of the collision. The probability of various inelastic processes is proportional to the probability that the struck electron end in a particular excited bound or continuum state. The peak of the inelastic energy loss is that for Compton scattering from a free electron at rest. The effect of the binding is reflected by a smearing of energy transfers about this mean due to the distribution of initial momenta of the bound electrons. Applied to the nucleus, we can similarly plot the difference in energy transfer of the meson in elastic scattering through angle θ by a stationary nucleus and by a stationary nucleon. This is plotted in Fig. 9. For momentum transfers where the struck nucleon would have final momentum corresponding to already occupied states, the Pauli principle would greatly modify the results, but it would be expected to be roughly correct for large-enough predicted energy transfers.

TABLE V. Uncorrected differential elastic cross sections for aluminum in millibarns per steradian.

θ_{lab}(deg)	$d\sigma/d\Omega$	θ_{lab}(deg)	$d\sigma/d\Omega$
20±3.2	512±47	65±5.7	7.52±0.75
25±3.2	293±26	70±5.7	8.08±0.94
30±3.2	202±17	75±5.7	4.78±0.73
35±3.2	125±13	80±5.7	6.10±0.63
35±3.9	117±11	85±5.7	3.38±0.44
40±3.9	78.0±9.0	90±5.7	1.99±0.53
45±3.9	38.1±4.1	95±5.7	1.38±0.43
50±3.9	18.7±3.1	100±5.7	1.85±0.51
50±5.7	17.8±2.2	105±5.7	1.89±0.50
55±5.7	11.2±1.6	110±5.7	1.91±0.42
60±5.7	8.55±0.75		

B. Comparison with Electron Scattering

In interpreting these results for carbon, it is of interest to examine Fregeau's results for the scattering of 187-Mev electrons.[17] These had momenta roughly the same as the 170 Mev/c momentum of the mesons used here. We note that, for a given scattering angle, the momentum transfer is essentially the "elastic" value, $2P_0 \sin(\theta/2)$, whether the nucleus is left in the ground state or in an excited state of $\lesssim 15$ Mev. In the impulse approximation, one regards the entire momentum transfer as being given to a single nucleon within the nucleus. The relative probability of the nucleus being found in its ground state, or various excited states, is then determined by the probability intensities for various final nuclear states when the struck-nucleus wave function is expanded in terms of the nuclear ground and excited states. The amplitude contribution

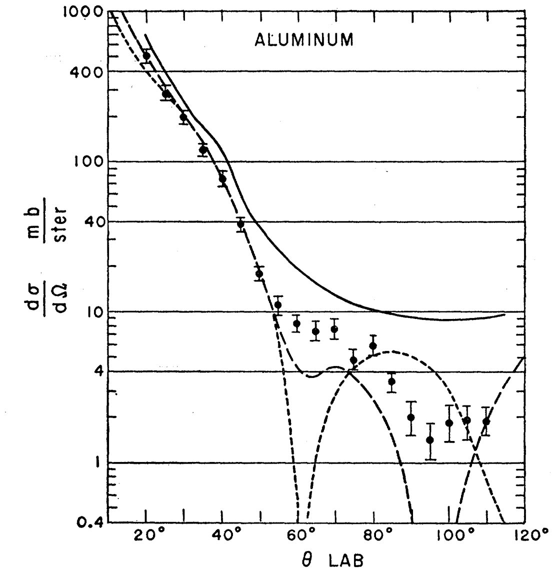

FIG. 7. 80-Mev π^- aluminum scattering. Solid curve is experimental result of Pevsner *et al.*[1] Dotted curve is from square well model, $V=-30-22i$ Mev.[4] Dashed curve is result of a modified Kisslinger model calculation with $R_0=1.08A^{\frac{1}{3}}\times10^{-13}$ cm, $a=0.25\times10^{-13}$ cm, $C=-1.1-0.2i$, and $C'=+0.35-0.25i$. Points are data of this experiment.

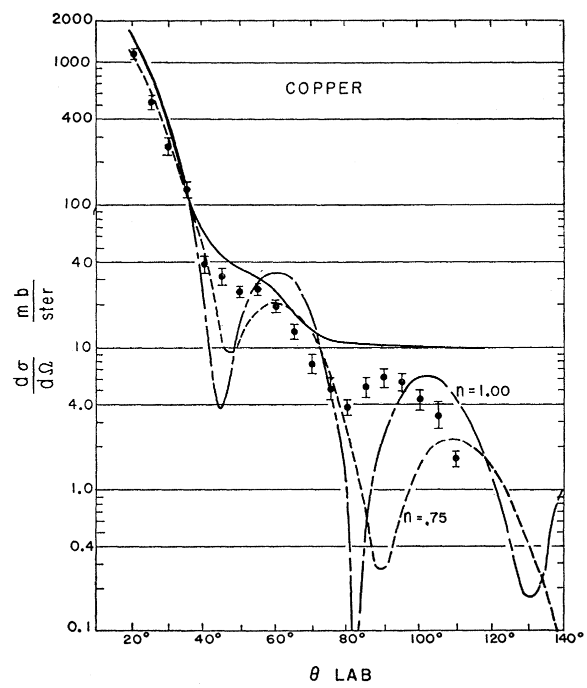

FIG. 8. 80-Mev π^- copper scattering. Solid curve is experimental result of Williams *et al.*[3] Dashed curves are from a square well model, $V=-35-20i$ Mev, with surface term.[3] Points are data of this experiment.

TABLE VI. Uncorrected differential elastic cross sections for copper in millibarns per steradian.

θ_{lab}(deg)	$d\sigma/d\Omega$	θ_{lab}(deg)	$d\sigma/d\Omega$
20±3.7	1140±88	65±4.7	14.8±3.0
25±3.7	525±62	65±6.0	12.1±2.1
30±3.7	258±32	70±6.0	7.69±1.14
35±3.7	129±16	75±6.0	5.19±0.89
40±4.7	38.4±5.3	80±6.0	3.82±0.42
45±4.7	31.9±4.1	85±6.0	5.30±0.81
50±4.7	24.7±1.9	90±6.0	6.16±0.86
55±4.7	24.6±2.5	95±6.0	5.78±0.80
55±6.0	29.0±5.7	100±6.0	4.33±0.67
60±4.7	20.5±2.9	105±6.0	3.36±0.66
60±6.0	17.9±3.3	110±6.0	1.65±0.21

from each nucleon to a particular final state must be summed. For a given momentum transfer, the ratio of neutron to proton excitation, and spin-flip to nonspin-flip contributions should be the free parameters remaining to determine the ratio of elastic scattering to inelastic scattering corresponding to the excitation of particular excited nuclear states. Although the electron scattering is primarily due to Coulomb interaction with the protons, there is also a contribution from the neutron and proton magnetic moments. The $T=\frac{3}{2}$, $j=\frac{3}{2}$, $l=1$ state is most important in pion-nucleon scattering at this energy, so the π^--neutron scattering is most important. Since carbon is symmetric in neutrons and protons, the electron and pion scattering might be expected in this argument to give the same ratio of elastic scattering to inelastic scattering to excited states which have strong matrix elements for excitation by this means.

The ratio (to the elastic cross section) of the partial cross sections for excitation of the 4.43-Mev, 7.65-Mev, and 9.61-Mev levels *versus* θ for 187-Mev electrons on

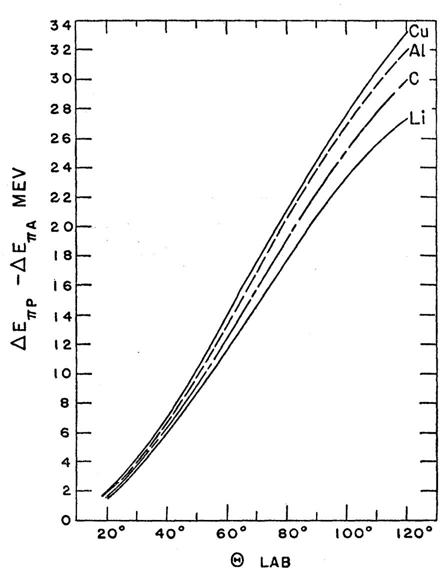

FIG. 9. Energy loss in an elastic collision of a pion with a nucleon at rest in the nucleus.

carbon are plotted in Fig. 10. The excitation of the 7.65-Mev level is weak in this region. There is a contribution of unresolved levels on the high-energy side of the 9.6-Mev level to ~12 Mev, with little further contribution until >15 Mev. The 9.6-Mev level contribution is larger than the others. Thus the "elastic," "5-Mev inelastic," and "10-Mev inelastic" scattering (for electrons) would be identified, respectively, with elastic scattering and (mainly) excitation of the 4.43- and 9.61-Mev levels. If we assume that the same is true for the meson scattering and plot the similar ratios for the case of π^- scattering for the corresponding

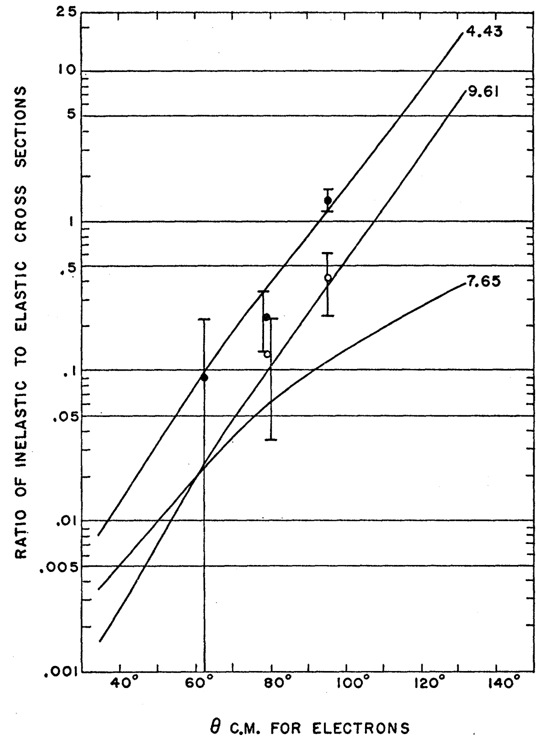

FIG. 10. Ratios of inelastic cross sections to elastic for excitation of levels in carbon by electron scattering (Fregeau[17]). ● Ratio for 5-Mev inelastic pion scattering, and ○ 10-Mev inelastic pion scattering at angle corresponding to same momentum transfer.

momentum transfer in the center-of-mass system, the points indicated in Fig. 10 are obtained. The 5- and 10-Mev inelastic scattering is small compared to the elastic scattering except at 110°, where the 5-Mev inelastic scattering is about 1.5 times the elastic scattering, and where the 10-Mev inelastic is about 0.5 times the elastic scattering. This corresponds to the ratios at 98° for the electron scattering case and 111° center-of-mass angle for the meson scattering. Thus the ratios agree to within experimental uncertainties for equal momentum transfer.

C. Comparison with Other Types of Scattering

The agreement above becomes much poorer if we compare the meson scattering with the scattering by fast nucleons or deuterons or α particles. More complicated possibilities enter in these cases, however. A single example is that the entering particles may remain after knocking out similar already present nucleons. Others include compound nucleus effects.

1. In the scattering of 96-Mev protons by carbon, Strauch and Titus[18] observed excitation of the 4.43- and 9.61-Mev levels but saw no evidence of the 7.68-Mev level. Their data show that for the ratio of the cross section for excitation of the 4.43-Mev level to the elastic cross section to be $\sim$1.5, the momentum transfer is $\sim$400 Mev/c, compared to 280 Mev/c for the electron and pion cases. The proton $cp=435$ Mev, compared to 170 and 187 Mev for the pion and electron cases.

2. In the scattering of 22-Mev alpha particles[19] ($cp=406$ Mev) by carbon, the 7.68-Mev level was observed in addition to the 4.4- and 9.6-Mev levels but down by factors of 10.7 and 8.2, respectively, relative to the latter levels for 233 Mev/c momentum transfer, with a decreasing ratio for higher momentum transfer. The ratio of 4.43-Mev excitation to elastic scattering at 90° shows considerable fluctuation with energy between 20.4- and 22.5-Mev bombarding energy, suggesting more complicated effects. Strong effects are seen from levels at 10.8, 11.1, and 11.74 Mev.

3. Haffner's[20] results for 15-Mev deuteron scattering ($cp=237$ Mev) for C^{12} for 220 Mev/c momentum transfer gives a ratio 0.25 for the 4.43-Mev excitation to elastic cross section. This compares with 0.20 for the electron scattering results for the same momentum transfer. The results are not presented in a manner favorable for a more detailed comparison of this type.

Because of the many excited levels[21] of Li^7 the various inelastic meson cross sections can not be assigned to excitation of specific states. As previously stated, we attribute the measured elastic cross section to true elastic scattering and excitation of the 0.48-Mev level. This is justified by the large gap between this first level and the second at 4.61 Mev. For 187-Mev electron scattering, the Stanford group detected the 0.48-Mev level as a broadening of the elastic peak.[22] From a comparison with the elastic peak for Li^6, which has its first level at 2.19 Mev, they estimate the cross section for excitation of the 0.48-Mev level to be about 10% of that for elastic scattering. In the meson scattering case therefore we expect the measured elastic cross section, $(d\sigma/d\Omega)_0$, to be due principally to true elastic scattering.

[18] K. Strauch and F. Titus, Phys. Rev. **103**, 200 (1956).

[19] Rasmussen, Miller, and Sampson, Phys. Rev. **100**, 181 (1955).

[20] J. W. Haffner, Phys. Rev. **103**, 1398 (1956).

[21] See F. Ajzenberg and T. Lauritsen, Revs. Modern Phys. **27**, 77 (1955) for a review of experiments on the level structure of light nuclei.

[22] J. F. Streib, Phys. Rev. **100**, 1797 (1955).

2. Elastic Scattering Comparison with Model Calculations

In the paper of Pevsner and Rainwater[4] and in that of Williams *et al.*,[3] optical model phase shift calculations were made for aluminum and copper, respectively, using a complex square well for the meson nuclear potential and matching at the nuclear surface with the suitable Coulomb wave function outside. Using a nuclear radius $R=1.4A^{\frac{1}{3}}\times10^{-13}$ cm and well depths from 0 to -45 Mev, they were able to get good agreement with their experimental results at small angles, but the prominent diffraction structure predicted was not then visible.

For 80-Mev π^- scattering from aluminum, Pevsner and Rainwater favor a nuclear well depth of $V_1=-30$ to -34 Mev and V_2 between -10 and -25 Mev to compare with their data at angles less than 50° (where $V=V_1+iV_2$). The result of their phase shift calculations for $V_1=-30$ and $V_2=-22$ Mev is shown in Fig. 7, together with their experimental results and those of this experiment. Agreement is good at angles of 50° and smaller.

Williams *et al.*[3] performed similar calculations for copper but in addition considered the surface term in the potential first suggested by Kisslinger.[23] Values of n of 0.50, 0.75, and 1.00 were used in matching the derivative of the wave function at the nuclear surface, where

$$\left.\frac{d\psi_l}{dr}\right|_+ = n\left.\frac{d\psi_l}{dr}\right|_- .$$

On the basis of a comparison with their data at small angles, they preferred a potential $V=(-35-20i)$ Mev. Figure 8 shows the calculated results for n values of 1.00 and 0.75. Rough agreement is obtained at angles $\leq 40°$.

In all cases of comparison the experimental cross sections at angles greater than about 50° are considerably different from the predictions of the complex square well calculations. It was expected that the predicted cross sections could be reduced at larger angles by ascribing a diffuse edge to the nucleus. This has been shown in the work of Saxon *et al.*[24,25] on nucleon scattering.

The lithium results show the elastic cross sections at angles above the minimum at $\sim$70° to be somewhat smaller than predicted by the experimental results and theoretical calculations of Williams *et al.*[2] Their calculations coherently combine the individual pion nucleon interactions for scattering from nucleons which remain in their same states in a nuclear harmonic oscillator well. They show that when the nuclear radius of $1.28A^{\frac{1}{3}}\times10^{-13}$ cm which they used is increased by about 10%,

[23] L. S. Kisslinger, Phys. Rev. **98**, 761 (1955).

[24] R. D. Woods and D. S. Saxon, Phys. Rev. **95**, 577 (1952).

[25] Melkanoff, Moszkowski, Nodvik, and Saxon, Phys. Rev. **101**, 507 (1956).

the backward-angle cross section is decreased somewhat, but the decrease is not sufficient to agree with the present results. Theoretical calculations, using an IBM-650 computer, of the elastic scattering from carbon are described in the following paper. A diffuse-edge nucleus was assumed with a nuclear density distribution

$$\rho(r)=\rho_0 f(r)=\rho_0\left[1+\exp\left(\frac{r-R_0}{a}\right)\right]^{-1},$$

where $R_0=r_0A^{\frac{1}{3}}$, and ρ_0 is the nucleon density at the center of the nucleus.

It was not possible to fit the data with an interaction of the V_1+iV_2 type, although various values of these parameters as well as r_0 and a were used.

An interaction of the Kisslinger type, which takes into account the p-wave as well as the s-wave nature of the scattering from single nucleons, was used. The meson wave equation becomes

$$\nabla^2\psi+k_0^2\psi=(1+Cf)^{-1}\{k_0^2[(C+C')f+U_C]\psi-C\nabla f\cdot\nabla\psi\},$$

where ψ is the meson wave function and k_0 the outside wave number. C' and C are, respectively, related to the s and p wave portions of the coherent average single nucleon scattering amplitudes. The real part of C is negative and $\lesssim -1$ so $(1+Cf)$ changes the sign of the right side within the nucleus if taken in this form. This is the Kisslinger[23] model. We have mainly used a "modified Kisslinger" model obtained by replacing $(1+Cf)^{-1}$ by $(1-Cf)$ for reasons discussed in the following paper. U_C is a relativistic Coulomb term. The best match which we have obtained for carbon, shown in Fig. 5, is with a modified Kisslinger theory using $R_0=1.08A^{\frac{1}{3}}\times10^{-13}$ cm, $a=0.25\times10^{-13}$ cm, $C=-1.1-0.1i$, and $C'=+0.35-0.15i$. Well over 100 choices of parameters were tried for various models as discussed in more detail in the following paper. The fit for carbon is considered to be particularly satisfying. The value of a is half of that favored by electron scattering. The best parameters for the other elements are shown in the captions to the figures.

ACKNOWLEDGMENTS

The authors wish to express their gratitude to those at the Nevis Cyclotron Laboratories who made this experiment possible. They want particularly to thank the cyclotron operators not only for operating the accelerator but also for assistance in recording the data.

The Radio Corporation of America is thanked for providing financial assistance (for W.F.B.) and for some of the equipment used in this research.